Potential of Martensitic Stainless Steel X5CrNiCuNb 16-4 as Pipe Steel in Corrosive CCS Environment

Anja Pfennig and Axel Kranzmann

Abstract—**Pipe steels suitable for carbon capture and storage technology (CCS) require resistance against the corrosive environment of a potential CCS-site (heat, pressure, salinity of the aquifer, CO_2-partial pressure). X5CrNiCuNb16-4 has been proven to be sufficient resistant in corrosive environments, but shows rather unusual corrosion behaviour in CCS environment. Therefore differently heat treated coupons of 1.4542 were kept at T=60 °C and ambient pressure as well as p=100 bar for 700 h - 8000 h in an a) water saturated supercritical CO_2 and b) CO_2-saturated synthetic aquifer environment similar to on-shore CCS-sites in the Northern German Basin. Additionally fatigue tests were performed via push-pull tests with a series of 30 specimens was tested at stress amplitudes between 150 MPa and 500 MPa (sinusoidal dynamic test loads, R=-1; resonant frequency ~ 30 Hz). Best corrosion resistance in the liquid phase is achieved via normalizing prior to exposure and hardening+tempering at 670 °C leads to lowest corrosion rates in the supercritical phase. With no regard to atmosphere discontinuously ellipsoidal surface corrosion regions appear after exposure of 4000 h and more. The endurance limit of X5CrNiCuNb16-4 measured in air is reduced by more than 50% when exposed to CCS environment (maximum number of cycles (10×10^6) at a stress amplitude of 150 MPa) The scatter range TN = 1:34 is disproportionately large contributing to an overall unusual corrosion behaviour**

Index Terms—**Corrosion, CCS, carbon storage, aquifer, heat treatment, fatigue, endurance limit.**

I. Introduction

During the compression of emission gasses e.g. from combustion processes of power plants into deep geological layers of a geological on-shore saline aquifer CCS-site (CCS Carbon Capture and Storage [1], [2]), the corrosion of injection pipe steels may become an issue when are compressed [3]-[9]. CO_2-corrosion is sensitively dependent on
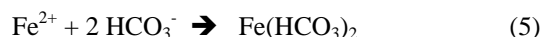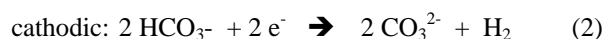
- alloy composition,
- contamination of alloy and media,
- temperature,
- CO_2 partial pressure,
- flow conditions
- protective corrosion scales [5], [6], [10]-[21].

Alloying elements [22] as well as heat treatment (temperature and time of austenitisizing, cooling rate as well

as temperature and time of annealing [23]-[25]) shows significant influence upon the corrosion resistance of steels, e.g. high Ni- and Cr contents [26], [27] improve general corrosion resistance as well as retained austenite improves pitting corrosion resistance [26]. Higher austenitizing temperature of martensitic steels [28]-[30] as well as higher annealing temperature of lean duplex stainless steels [22], [23], [28] decrease the pitting potential. Due to reactive grain boundaries in martensitic microstructure C-Mn (carbon) steels in a H_2S-containing NaCl solution shows higher corrosion rates than ferritic or ferritic-bainitic microstructures [31].

Corrosion phenomena were also found to be reason for early failure of materials under cyclic load [32]-[34]. Pit formation on stainless steels is enhanced by chemical reactions, local changes of lattice energy within the steel`s surface and mechanical load [35], [36]. Higher grain/phase boundary energy where dual or triple points of grain/phase boundaries occur enhances crack initiation and accelerates crack propagation [32], [34]. This local lattice mismatch also initiates pit -, selective - and inter granular corrosion that lead to crack formation [33]. A possible crack initiation model was presented by Han *et al.* [37] and modified by Pfennig *et al.* [35], [36] (Fig. 1).

Surface corrosion layers grow slowly and locally corroded samples usually show the same corrosion products as surface layers [15], [17], acting as corrosion catalyser. Generally siderite $FeCO_3$ [3], [38] is formed on steels exposed to CO_2-environment (a) due to the low solubility of $FeCO_3$ in water ($p_{Ksp} = 10.54$ at 25 °C [29], [37]) leading to anodic iron dissolution. The initial formation of transient $Fe(OH)_2$ [6], [30] (grey area in: a) possibly leads to an increase of the local pH near the hydroxide film. As a consequence an internal and external ferrous carbonate film precipitates, Han *et al.* [37] (a and b) according to equations 1 to 6 [15], [29]:

$$CO_2 \, (g) + H_2O \, (l) \quad \longrightarrow \quad H^+ + HCO_3^- \, (aq) \qquad (1)$$

$$\text{cathodic: } 2\,HCO_3^- + 2\,e^- \quad \longrightarrow \quad 2\,CO_3^{2-} + H_2 \qquad (2)$$

$$\text{anodic: } \qquad Fe \quad \longrightarrow \quad Fe^{2+} + 2e^- \qquad (3)$$

$$Fe^{2+} + CO_3^{2-} \longrightarrow FeCO_3 \qquad (4)$$

$$Fe^{2+} + 2\,HCO_3^- \longrightarrow Fe(HCO_3)_2 \qquad (5)$$

$$Fe(HCO_3)_2 \quad \longrightarrow \quad FeCO_3 + CO_2 + H_2O \qquad (6)$$

The internal and external corrosion layer grow depending on the various carbon and oxygen partial pressures (b). Local damage of the ferrous hydroxide film (c) due to mechanical and/or chemical effects exposes the highly porous non-protective ferrous carbonate to the geothermal water with lower pH. The ferrous carbonate film begins to dissolve

and depassivate the steel (d). Local surface degradation is enhanced because oxygen vacancies consolidate and condense at the hydroxide/brine interface and detach the siderite from the hydroxide film in lateral direction in direction of the applied mechanical stress (e). The flowing corrosive media removes the remaining film causing the pit to grow wider, because the same steps will occur from the beginning on the newly exposed surface (f). Simultaneously crack propagation will take place due to the dynamic load and forces at the pit bottom, because the stress concentrations and plastic deformation lead to the production of slip bands [26] highly susceptible to the corrosion explained. The crack flanks are immediately wetted repeating the corrosion steps within the crack itself.
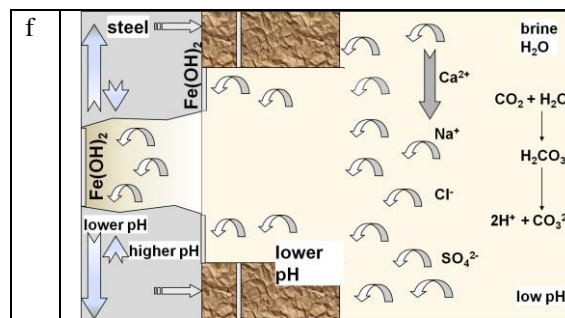

Fig. 1. Possible crack initiation mechanism (schematic).

II. EXPERIMENTAL PROCEDURE

A. Material

Static corrosion tests as well as corrosion fatigue tests were carried out using heat treated samples of martensitic AISI 630 (X5CrNiCuNb16-4, 1.4542 (Table I) and (Table II).

TABLE I: CHEMICAL COMPOSITION OF 1.4542 (X5CRNICUNB16-4, AISI 630), NO CO DETECTED

Elements	C	Si	Mn	P	S	Cr
acc standard [a]	≤ 0.07	≤ 0.70	≤ 1.50	≤ 0.04	≤ 0.015	15.0 - 17.0
analysed [b]	0.03	0.42	0.68	0.018	0.002	15.75
Elements	**Mo**	**Ni**	**Cu**	**Nb**	**Fe**	
acc standard [a]	≤ 0.60	3.00 – 5.00	3.00 – 5.00	0.20 – 0.45	rest	
analysed [b]	0.11	4.54	3.00	0.242	75.00	

[a] Elements as specified according to **DIN EN 10088-3 in %**
[b] Spark emission spectrometry

TABLE II: HEAT TREATMENT PROTOCOL FOR X5CRNICUNB16-4

heat treatment	temperature ℃ / ℃	time min	cooling medium
normalizing	850	30	oil
hardening	1040	30	oil
hardening + tempering 1, 600 ℃	1040 / 550	30	oil
hardening + tempering 2, 670 ℃	1040 / 650	30	oil
hardening + tempering 3, 700 ℃	1040 / 755	30	oil

To simulate in-situ geothermal condition the geothermal quifer water (as known to be similar to the Stuttgart Aquifer [39]: Ca^{2+}: 1760 mg/L, K^{2+}: 430 mg/L, Mg^{2+}: 1270 mg/L, Na^{2+}: 90,100 mg/L, Cl^-: 143,300 mg/L, SO_4^{2-}: 3600 mg/L, HCO_3^-: 40 mg/L) was synthesized in a strictly orderly way to avoid precipitation of salts and carbonates.

B. Static Experiments

Laboratory scale exposure tests in CO_2-saturated aquifer brine and water saturated CO_2 were carried using coupons of the steel quality X5CrNiCuNb16-4 (1.4542) may be used as injection pipe using samples made of thermally treated specimen of steels with 8 mm thickness, 20 mm width, 50 mm length. Heat treatment to gain martensitic microstructure with sufficient hardness and toughness prior to exposure was done following commonly used protocols according to Table II:

A hole of 3.9 mm diameter was used for sample positioning. Samples of each base metal were positioned
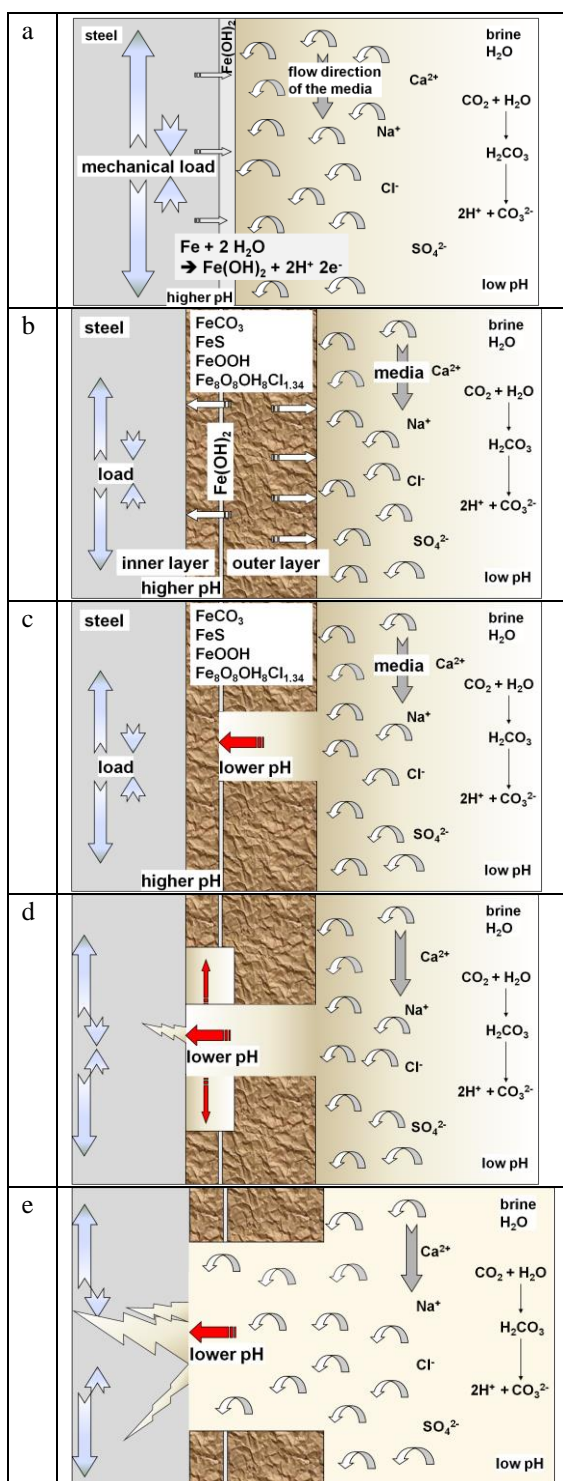
within the vapour phase and within the liquid phase. Flow control (3 NL/h) of the technical CO_2 (purity 99,995 vol.-%)) into the brine at ambient pressure was done by a capillary meter GDX600_man by QCAL Messtechnik GmbH, Munic. The exposure of the samples between 700 h to 8000 h was disposed in reaction vessels according to the conditions at the geological site at 60 °C at ambient pressure – each material in a separated reaction vessel [15], [40] and at 100 bar [41], [42] (Fig. 2).
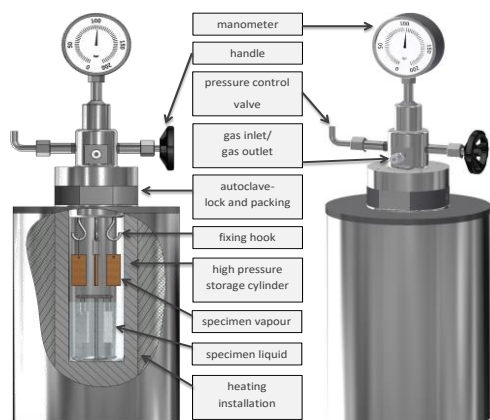

Fig. 2. Reaction vessels and experimental set up.

Before corrosion tests the surfaces of the steels were activated by grinding with SiC-Paper down to 120 μm under water. After the corrosion tests, the samples were cut partly for scale analysis with the corrosion layer and prepared partly for kinetic analysis after the scale was etched. Descaling of the samples was performed by exposure to 37% HCl. Then parts of the samples were embedded in a cold resin (Epoxicure, Buehler), cut and polished first with SiC-Paper from 180 μm to 1200 μm under water and then finished with diamond paste 6 μm and 1 μm.

C. Dynamic Experiments

An appropriate system for fatigue testing at temperatures existing in deep geological layers (in-situ conditions) was set up, to assess materials of components loaded cyclically and exposed constantly to the highly corrosive hot thermal water at 60 °C and ca. 20 % salinity of the geothermal water and fluid properties differing strongly [39]. Fatigue tests were carried out using samples of martensitic AISI 630 (X5CrNiCuNb16-4, 1.4542, tensile strength in air: 1078 MPa) (Table I). The surfaces were activated via machining to Rz=4.

The objective was to simulate in-situ conditions (temperature 60 °C, corrosive environment) of a material exposed to dynamic mechanical stress and corrosive gas-saturated saline aquifer environment. The corrosion chamber is fixed directly onto the sample leaving the resonant testing machine unaffected (Fig. 3). During mechanical stress-strain tests a magnetically driven gear pump constantly pumps the corrosive media from the reservoir to the corrosion- and temperature-resistant corrosion chamber. The specimen is during the complete test surrounded of the corrosions medium. Heating is realized by a heating element which is placed at the reservoir. The ratio of sample surface to volume of the corrosive media after DIN 50905 Part 1 (10 ml/cm³) is greater than required. The connecting of the chamber onto

the specimen via clamping collar creates a force-fit process ensuring enough force to the corrosion chamber at high frequencies to keep it firmly on the test specimen. The corrosion chamber is sealed by O-rings made of Viton in the area of restraint. In order not to impede the change in length of the sample during the experiment, a membrane is applied to the corrosion chamber as a motion-compensating element. [41], [42].
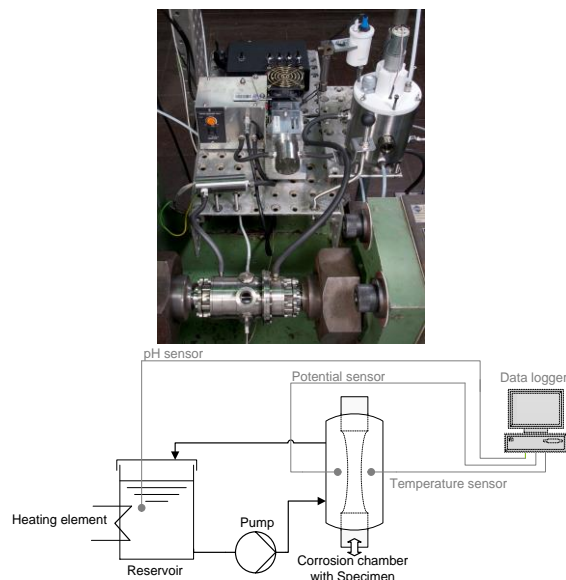

Fig. 3. Schematic set-up of operating corrosion chamber for in-situ corrosion fatigue testing [15], [40].

Electrochemical data were collected in the corrosion chamber during the mechanical tests along with temperature, pH and electrochemical potential. For measurement of the electrochemical potential a shock resistant silver-silver chloride electrode was fixed in a Teflon channel. To simulate non-static operation a resonant testing machine has been used at 30 – 40 Hz where samples of both steels were tested in stress-strain mode under CCS aquifer environment. In addition technical CO_2 was introduced into the closed system at a rate close to 9 L/h to keep stable environmental conditions.

The corrosion fatigue strength of stainless steel with16% chromium (X5CrNiCuNb16-4, 1.4542, hardened and tempered with martensitic microstructure) is examined in dynamic stress-strain tests in CO_2-saturated aquifer (Stuttgart Aquifer [40]) at 60 °C. Therefore a resonant testing machine (sinusoidal dynamic test loads, R=-1; resonant frequency ~ 30 Hz) has been used. In addition technical CO_2 was introduced into the closed corrosion chamber system at a rate close to 9 L/h to keep stable environmental conditions. In each test series 30 specimens were tested. X5CrNiCuNb16-4 was tested between 150 MPa and 500 MPa. Due to the rather heterogeneous fine machined surfaces (surface roughness Rz=4) the specimens are comparable with prefabricated parts.

D. Analysis

Different light optical and electron microscopy techniques were performed on specimens to investigate the layer structures and morphology of the samples. X-ray diffraction was carried out in a URD-6 (Seifert-FPM) with

CoKα-radiation with an automatic slit adjustment, step 0.03 ° and count 5 sec. Phase analysis was performed by matching peak positions automatically with PDF-2 (2005) powder patterns. Mainly structures that were likely to precipitate from the steels were chosen of the ICSD and refined to fit the raw-data-files using POWDERCELL 2.4 [43] and AUTOQUAN ® by Seifert FPM. To characterise the pitting corrosion, 3-D-images were realized by the double optical system Microprof TTV by FRT. Kinetics of the corrosion were determined by the corrosion rates which were calculated via mass change of the samples before and after corrosion testing according to DIN 50 905 part 1-4 and using the semi-automatic analyzing program Analysis Docu ax-4 by Aquinto.
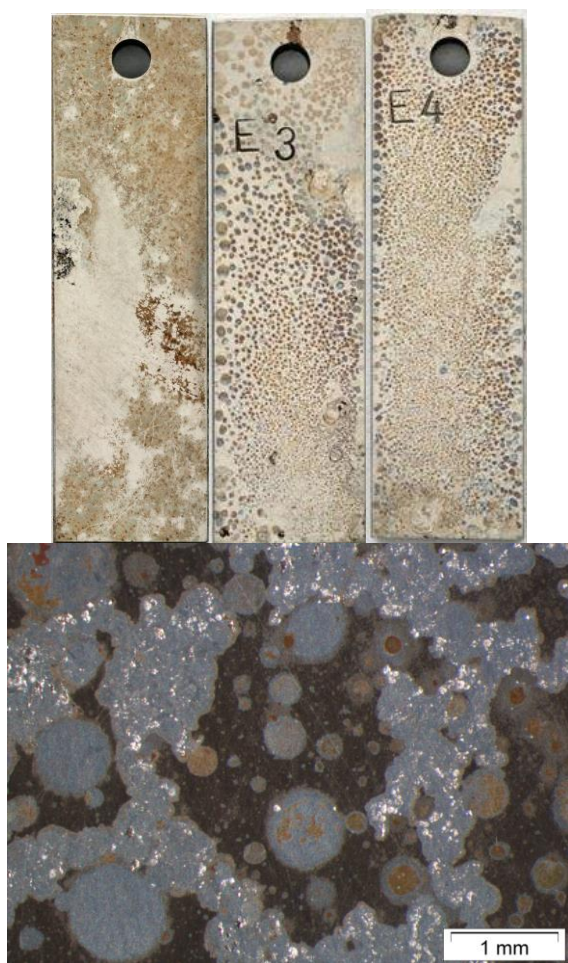

Fig. 4. Sample surfaces of X5CrNiCuNb16-4 hardened and tempered at 670 ℃ (E3) and 700 ℃ (E4) after 4000 h of exposure in water saturated supercritical CO_2 (upper left and middle) and CO_2-saturated brine (upper right).

III. RESULTS AND DISCUSSION

X5CrNiCuNb16-4 precipitates surface corrosion layers and pits when during CCS injection intermissions and reduced pressure in the injection pipe occur where the water level may rise within the pipe although in general the CO_2 is injected in its supercritical phase. This three phase boundary leads to an atmosphere, where surface corrosion results in a discontinuous layer structure described as "leopard" structure. This unusual corrosion formation is present in supercritical water saturated CO_2 even after short exposure times (700 h) (Fig. 4) and in CO_2-saturated brine after 4000 h of exposure

[42], [44]. Ellipsoidal regions of the sample surfaces are corroded visually while surrounding regions are protected by a passivating layer.

A. Kinetics of Static Corrosion Experiments

Samples exposed to water saturated supercritical CO_2 and CO_2-saturated brine do not reveal a distinct dependence on the heat treatment prior to exposure showing the same trends during the entire exposure time (Fig. 5). Maximum corrosion rate in the liquid phase is approximately 0.014 mm/year, after 8000 h and approximately 0.003 mm/year in the supercritical phase.

Corrosion rates obtained in supercritical CO_2 do not change as a function of time. But, long exposure times in CO_2-saturated brine lead to increasing surface corrosion rates after 4000 h due to a possible break-down of the initial passivating layer formed after 1000 h of exposure. This may be due to increasing carbide precipitation depleting the metal matrix of chromium and therefore prohibiting further surface passivation.
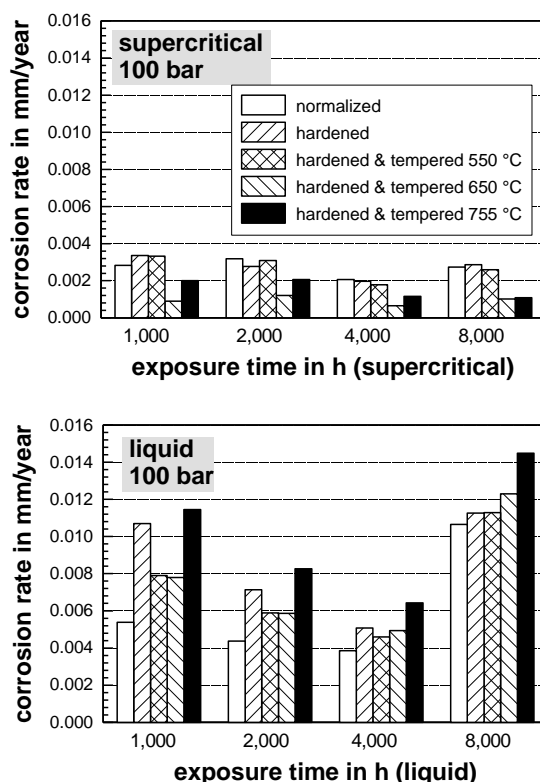

Fig. 5. Influence of heat treatment on the corrosion rate of 1.4542 in water saturated supercritical CO2 (top) and CO2 saturated saline aquifer water (bottom [42], [44]) at 60 °C and 100 bar.

Due to passivation X5CrNiCuNb16-4 shows very low corrosion rates in water saturated supercritical CO_2 depending either on the lack of electrolytes [42] or more possible on the cathodic reaction described in equation (1) leading to a higher H_2CO_3 concentration and therefore more acidic and reactive environment as in the CO_2 saturated liquid phase [7], [26]. In CO_2-containing water carbonic acid is formed due to the low pH and because the solubility of iron carbonate $FeCO_3$ is low [29] siderite forms. In general, the leopard shaped corrosion layer reveals siderite $FeCO_3$ and goethite a-FeOOH as precipitation phases.

Two explanations are possible for the "leopard shape":
1) Carbides are more susceptible to corrosion initiation [27],

[42] and therefore the passivation of the steel surface is locally destroyed where carbides precipitated.

2) In water saturated supercritical CO_2 at 100 bar and 60 ℃ the decreasing water solubility in the supercritical carbon dioxide [26] leads to wetting of the metal surface via very thin and small water droplets. Because time was too short to precipitate pits the typical "leopard" shaped corrosion layer is formed indicating the initial droplets on the surface [42]. Areas of former droplets consolidate resulting in small pits surrounding the former droplet (Fig. 4) containing sulphates ($FeSO_4$) in the outer areas whereas the center shows hematite (Fe_2O_3) (Fig. 6).
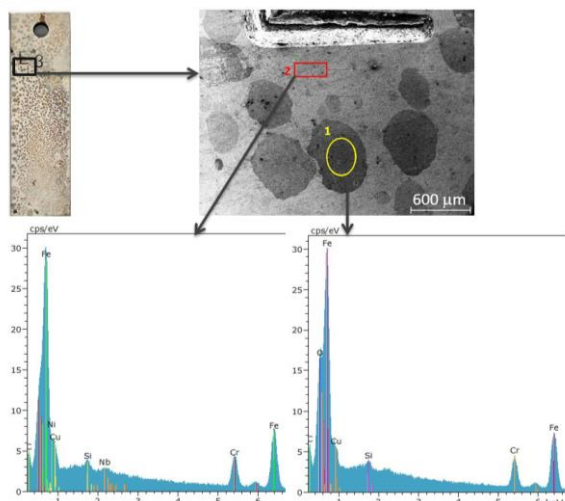

Fig. 6. SEM micrographs and element distribution of the ellipsoidal corrosion layer formed on 1.4542 hardened and tempered at 670 ℃ prior to exposure after 8000 hours of exposure at 60 ℃ and 100 bar to water saturated supercritical CO_2.

The influence on heat treatment prior to exposure has been widely described [11], [22], [28], [29]. Under supercritical CO_2 conditions a martensitic microstructure of hardened and tempered 1.4542 at low temperatures (650 ℃) (< 0.001 mm/year) and under saline water normalized microstructure (ca. 0.004 mm/year) offer best corrosion resistance regarding surface corrosion (Fig. 5) [42]. Independent of the heat treatment X5CrNiCuNb16-4 developed a rather high number of pits per m² in both atmospheres, water saturated supercritical CO_2 and CO_2 saturated aquifer water (Fig. 7). The number of pits precipitated in the supercritical phase is approximately ten times higher than in the liquid phase. Heat treatment hardening and tempering that showed highest surface corrosion resistance reveals now the greatest number of pits (Fig. 7, top). Pit depths measured after exposure at 100 bar and 60 ℃ are about 10-250 μm.

B. Corrosion Fatigue Behaviour

The unusual corrosion phenomena of X5CrNiCuNb16-4 are accompanied by an also unusual corrosion fatigue behavior described by Pfennig *et al.* [41], [42]. The S-N-curve did not show typical fatigue strength (Fig. 8). The large scatter range TN=1:34, the possibility of an influence of three different charges of aquifer water [45] and the very small coefficient of correlation r² = 0.33 indicate a non-linear relationship of the considered variables giving only a 24% chance of linear relationship. The corrosion fatigue strength of X5CrNiCuNb16-4 is 60% below the endurance limit

measured in air (620 MPa). Maximum number of cycles (10×10^7) was reached at a stress amplitude of 150 MPa. The decrease of the fatigue limit line with increasing number of cycles (Wöhler-exponent of k = 3.59) is much larger in corrosive environment than in air [41].
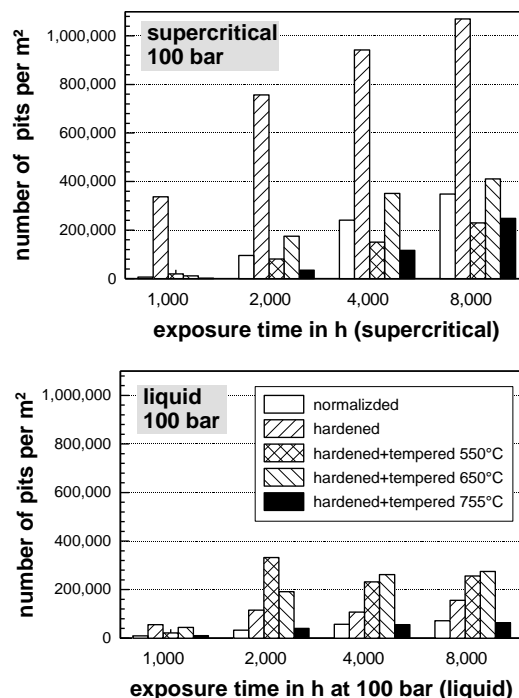

Fig. 7. Influence of heat treatment on the local corrosion of 1.4542 in water saturated supercritical CO_2 (top) and CO_2 saturated saline aquifer water (bottom [42], [44]) at 60 °C and 100 bar.
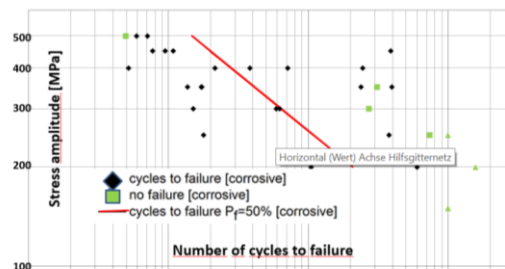

Fig. 8. S-N-curve and sample of 1.4542 exposed to flowing saline aquifer [40] and CO2 at 60 ℃ [41], [45].
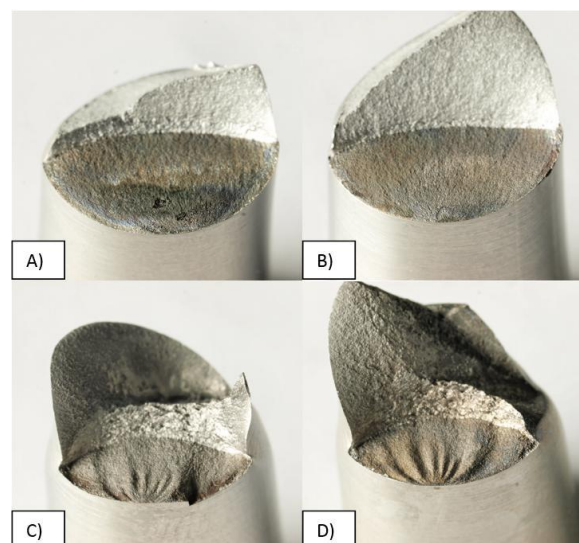

Fig. 9. Crack surfaces after fatigue failure. Samples reveal impurities with no influence on endurance limit.
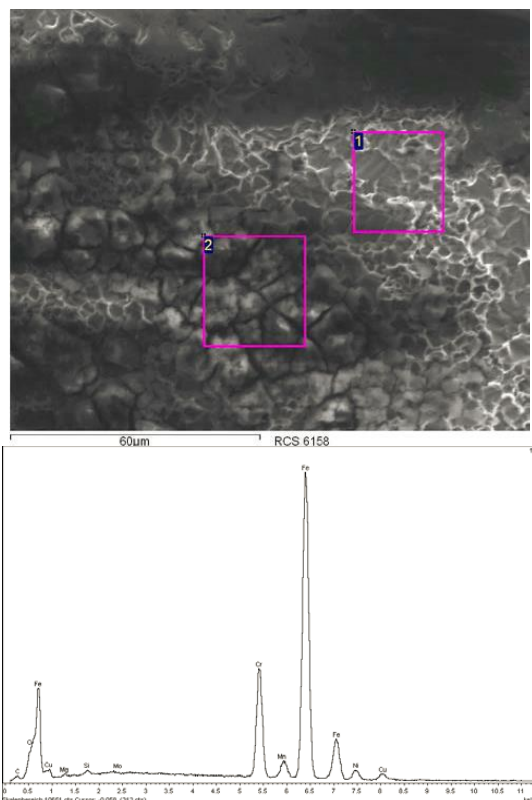
Fig. 10. Surface image (left) of corrosion layer on crack flank and main elements indicating Al as impurity (right). Element distribution revealing contaminants of the samples.

Local corrosion is enhanced within the microstructure as a result of chlorides [46] and increased dislocation number, grain boundaries, boundaries of precipitation phases e.g. carbides leading to local lattice mismatch resulting in higher local boundary energy [47]. Multiple cracks found throughout the entire sample area of X5CrNiCuNb16-4 initiated from pits are responsible for early failure. Impurities were found on various surfaces with no significant correlation to the endurance limit (Fig. 9). Surfaces revealed corrosion layers mainly composed of iron carbonate (siderite, $FeCO_3$) and iron hydroxide ($Fe(OH)_2$) (Fig. 10). Both, the presence and the thickness of the corrosion layer could not be related to early failure. The number of striations indicating the opening and closing of the initial crack during cyclic load was also not a matter of early or late failure.

After hardening and annealing the microstructure of X5CrNiCuNb16-4 reveals the typical needle-structure of martensite with embedded δ-ferrite. Samples with short number of cycles to failure contained Al within the corrosion layer (Fig. 10) and revealed non-metallic inclusions that were ordered discontinuously lamellar within the alloy. It may be assumed that, impurities such as Al present in the base material may consolidate during cyclic loading within corrosive environment and then lead to unpredictable early failure.

IV. CONCLUSION

Corrosion rates, local corrosion accompanied with crack initiation are decisive when deciding if the steels are suitable for CCS application. Steels will be unsuitable for its use in pressure vessel applications if the corrosion rate exceeds 0,1 mm/year. Neither aquifer water, microstructure of X5CrNiCuNb16-4 nor mechanical properties such as hardness or distinct crack propagation were proved to be of influence on mechanical properties. Crack formation is correlated with pit corrosion phenomena resulting in inter crystalline corrosion. It may also be possible that these impurities lead to local corrosion phenomena, but again failure is not necessary a consequence of local corrosion. Therefore Al is the only significant evidence for lower endurance limits. However, this still does not fully explain the unusual corrosion and corrosion fatigue behavior of the metal. Reliable corrosion rates and lifetime predictions regarding pit corrosion and corrosion fatigue for X5CrNiCuNb16-4 in CCS technology are not possible. A high sensitivity on a homogeneous microstructure upon the corrosion and corrosion fatigue behaviour of X5CrNiCuNb16-4 needs to be taken into account when regarding this steel as pipe steel during injection of CO_2 into saline aquifers. The following findings may be summarized:

- Surface Corrosion rates are lower in supercritical CO_2, but pit corrosion resistance is better in CO_2 saturated brine.
- "Leopard structured" surface corrosion is related to chemical decomposition, water and CO_2 partial pressure, presence of electrolyte, pH, and early pit formation
- $FeCO_3$ and FeOOH are corrosion products under static and dynamic corrosion tests
- No correlation could be found between the inclusions and early rupture although specimens with inclusions at the fracture surface and its cross section endured lower number of cycles.
- Al was analyzed in specimens with low number of cycles and may be cause for early rupture during corrosion fatigue tests.

REFERENCES

[1] D. C. Thomas, "Carbon dioxide capture for storage in deep geologic formations — Results from CO₂ capture project," *Capture and Separation of Carbon Dioxide form Combustion Sources*, 2005, vol. 1.

[2] M. Broek, R. Hoefnagels, E. Rubin, W. Turkenburg, and A. Faaij, "Effects of technological learning on future cost and performance of power plants with CO₂ capture, in projects costs of generating electricity," *Progress in Energy and Combustion Science,* pp. 177-187, 2011.

[3] S. Nešić, "Key issues related to modelling of internal corrosion of oil and gas pipelines — A review," *Corrosion Science,* vol. 49, pp. 4308–4338, 2007.

[4] S. Hurter, "Impact of mutual solubility of H₂O and CO₂ on injection operations for geological storage of CO₂," in *Proc. International Conference of the Properties of Water and Steem ICPWS*, Berlin, September 8-11.

[5] L. Zhang, J. Yang, J. S. Sun, and M. Lu, "Effect of pressure on wet H2S/CO2 corrosion of pipeline steel, no. 09565," in *Proc. NACE Corrosion 2008 Conference and Expo*, New Orleans, Louisiana, USA, March 16-20, 2008.

[6] L. J. Mu and W. Z. Zhao, "Investigation on carbon dioxide corrosion behaviors of 13Cr stainless steel in simulated strum water," *Corrosion Science*, pp. 1-24, 2009.

[7] M. Seiersten, "Material selection for separation, transportation and disposal of CO2," *NACE Corrosion*, 2001.

[8] Z. D. Cui, S. L. Wu, S. L. Zhu, and X. J. Yang, "Study on corrosion properties of pipelines in simulated produced water saturated with supercritical CO_2," *Applied Surface Science*, vol. 252, pp. 2368-2374, 2006.

[9] A. Pfennig and A. Kranzmann, "Reliability of pipe steels with different amounts of C and Cr during onshore carbon dioxide injection," *International Journal of Greenhouse Gas Control,* vol. 5, pp. 757–769, 2011.

[10] H. Zhang, Y. L. Zhao, and Z. D. Jiang, "Effects of temperature on the corrosion behaviour of 13Cr martensitic stainless steel during exposure to CO2 and Cl- environment," *Material Letters*, no. 59, pp. 3370-3374, 2005.

[11] J. N. Alhajji and M. R. Reda, "The effect of alloying elements on the electrochemical corrosion of low residual carbon steels instagnant CO_2-saturated brine," *Corrosion Science*, vol. 34, no. 11, pp. 1899-1911, 1993.

[12] Y.-S. Choi and S. Nešić, "Corrosion behaviour of carbon steel in supercritical CO2-water environments," in *Proc. 2008 Conference and Expo*, New Orleans, Louisiana, USA, March 16-20, 2008.

[13] X. Jiang, S. Nešić, and F. Huet, "The effect of electrode size on electrochemical noise measurements and the role of chloride on localized CO_2 corrosion of mild steel," in *Proc. NACE Corrosion 2008 Conference and Expo*, New Orleans, Louisiana, USA, March 16-20, 2008.

[14] Z. Ahmad, I. M. Allam, and B. J. Abdul Aleem, "Effect of environmental factors on the atmospheric corrosion of mild steel in aggressive sea coastal environment," *Anti Corrosion Methods and Materials*, no. 47, pp. 215-225, 2000.

[15] P. Fennig and R. Bäßler, "Effect of CO_2 on the stability of steels with 1% and 13% Cr in saline water," *Corrosion Science*, vol. 51, issue 4, pp. 931-940, 2009.

[16] A. Pfennig and A. Kranzmann, "The role of pit corrosion in engineering the carbon storage site Ketzin, Germany," *WIT Transactions on Ecology and the Environment*, vol. 126, 2010, pp. 109-118.

[17] P. Zastrow, A. Kranzmann *et al.*, "Influence of heat treatment on the corrosion behaviour of stainless steels during CO2-sequestration into saline aquifer," *International Journal of Green House Gas Control,* vol. 15, pp. 213–224, 2003.

[18] R. Nyborg, "Controlling internal corrosion in oil and gas pipelines," *Business Briefing: Exploration & Production: The Oil & Gas Review*, issue 2, pp. 70-74, 2005.

[19] D. S. Carvalho, C. J. B. Joia, and O. R. Mattos, "Corrosion rate of iron and iron-chromium alloys in CO_2-medium," *Corrosion Science,* no. 47, pp. 2974-2986, 2005.

[20] B. R. Linter and G. T. Burstein, "Reactions of pipeline steels in carbon dioxide solutions," *Corrosion Science,* no. 41, pp. 117-139, 1999.

[21] S. L. Wu, Z. D. Cui, G. X. Zhao, M. L. Yan, S. L. Zhu, and X. J. Yang, "EIS study of the surface film on the surface of carbon steel form supercritical carbon dioxide corrosion," *Applied Surface Science,* no. 228, pp. 17-25, 2004.

[22] Ş. Bülbül and Y Sun, "Corrosion behaviours of high Cr-Ni cast steels in the HCl solution," *Journal of Alloys and Compounds,* no. 598, pp. 143-147, 2010.

[23] B. Hou, Y. Li, Y. Li, and J. Zhang, "Effect of alloy elements on the anti-corrosion properties of low alloy steel," *Bull. Mater. Sci,* vol. 23, no. 3, pp. 189-192, 2000.

[24] Z. Cvijović and G. Radenković, "Microstructure and pitting corrosion resistance of annealed duplex stainless stell," *Corrosion Science,* vol. 48, pp. 3887-3906, 2006.

[25] J. Y. Park and Y. S. Park, "The effects of heat-treatment parameters on corrosion resistance and phase transformation of 14Cr-3Mo martensitic stainless steel," *Materials Science and Engineering,* pp. 449-451, pp. 1131-1134, 2007.

[26] J. Banaś, U. Lelek-Borkowska, B. Mazurkiewicz, and W. Solarski, "Effect of CO2 and H2S on the composition and stability of passive film on iron alloy in geothermal water," *Electrochimica Acta,* vol. 52, pp. 5704–5714, 2007.

[27] P. D. Bilmes, C. L. Llorente, C. M. Méndez, and C. A. Gervasi, "Microstructure, heat treatment and pitting corrosion of 13CrNiMo plate and weld metals," *Corrosion Science*, vol. 51, issue 4, pp. 876-882, 2009.

[28] L. Zhang, W. Zhang, Y. Jiang, B. Deng, D. Sun, and J. Li, "Influence of annealing treatment on the corrosion resistance of lean duplex stainless steel," 2101.

[29] B. Brown, S. R. Parakala, and S. Nešić, "CO_2 corrosion in the presence of trace amounts of H2S," *Corrosion, Paper,* no. 04736, pp. 1-28, 2004.

[30] A. N. Isfahany, H. Saghafian, and G. Borhani, "The effect of heat treatment on mechanical properties and corrosion behaviour of AISI420 martensitic stainless steel," *Journal of Alloys and Compounds*, no. 509, pp. 3931-3936, 2011.

[31] M. A. Lucio-Garciaa, J. G. Gonzalez-Rodrigueza, M. Casalesc, L. Martinezc, J. G. Chacon-Navaa, M. A. Neri-Floresa, and A. Martinez-Villafañea, "Effect of heat treatment on H2S corrosion of a micro-alloyed C–Mn steel," *Corrosion Science,* vol. 51, pp. 2380-2386, 2009.

[32] C. Madduri and R. V. Prakash, "Corrosion Fatigue Crack Growth Studies in Ni-Cr-Mn steels," *International Journal of Mechanical and Materials Engineering,* vol. 1, pp. 20-25, 2010.

[33] M. Seo, "Electrochemical society. Corrosion division, passivity and localized corrosion: An international symposium in honour of professor Norio Sato, initiation and stability of localized corrosion processes on stein steels," *The Electrochemical Society,* pp. 483-490, 1999.

[34] V. Vignal, O. Delrue, J. Peultier, and R. Oltra, "Critical factors in localized corrosion 5: A symposium in honour of Hugh Isaacs, local mechanical-electrochemical behavior of duplex stainless steels," *The Electrochemical Society*, pp. 102-104, 2007.

[35] A. Pfennig, M. Wolf, and T. Böllinghaus, "Corrosion fatigue of X46Cr13 in CCS environment, in energy technology 2016: Carbon dioxide management and other technologies," vol. 1, pp. 49-56, 2016.

[36] A. Pfennig, R. Wiegand, M. Wolf, and C.-P. Bork, "Corrosion and corrosion fatigue of AISI 420C (X46Cr13) at 60 ℃ in CO_2-saturated artificial geothermal brine," *Corrosion Science*, vol. 68, pp. 134–143, 2013.

[37] J. Han, Y. Yang, S. Nešić, and B. N. Brown, "Roles of passivation and galvanic effects in localized CO_2 corrosion of mild steel," in *Proc. NACE Corrosion 2008*, New Orleans, Louisiana, USA, March 2008.

[38] A. Pfennig, H. Wolthusen, P. Zastrow, and A. Kranzmann, "Evaluation of heat treatment performance of potential pipe steels in CCS-environment," *Carbon Dioxide Management and Other Technologies*, vol. 1, pp. 15-22, 2015.

[39] A. Förster, B. Norden, K. Zinck-Jørgensen, P. Frykman, J. Kulenkampff, E. Spangenberg, J. Erzinger, M. Zimmer, J. Kopp, G. Borm, C. Juhlin, C. Cosma, and S. Hurter, "Baseline characterization of the CO2SINK geological storage site at Ketzin," *Germany: Environmental Geosciences,* vol. 13, no. 3, pp. 145-161, September 2006.

[40] M. Wolf, R. Afanasiev, T. Böllinghaus, and A. Pfennig, "Investigation of corrosion fatigue of duplex steel X2CrNiMoN22 5 3 exposed to a geothermal environment under different electrochemical conditions and load types," in *Proc. 13th International Conference on Greenhouse Gas Control Technologies*, pp. 14-18, November 2016, Lausanne, Switzerland.

[41] A. Pfennig, K. Heynert, M. Wolf, and T. Böllinghaus, "First in-situ electrochemical measurement during fatigue testing of injection pipe steels to determine the reliability of a saline aquifer water CCS-site in the Northern German basin original," *Energy Procedia*, vol. 63, pp. 5773-5786, 2014.

[42] A. Pfennig, H. Wolthusen, and A. Kranzmann, "Unusual corrosion behavior of 1.4542 exposed a laboratory saline aquifer water CCS-environment," *GHGT13*, 2016, Lausanne, Switzerland.

[43] S. W. Kraus and G. Nolze, "Powder cell — A program for the representation and manipulation of crystal structures and calculation of the resulting X-ray powder patterns," *J. Appl. Cryst.,* vol. 29, pp. 301-303, 1996.

[44] A. Pfennig, H. Wolthusen, M. Wolf, and A. Kranzmann, "Effect of heat treatment of injection pipe steels on the reliability of a saline aquifer water CCS-site in the Northern German basin," *Energy Procedia,* vol. 63, pp. 5762-5772, 2014.

[45] A. Pfennig, M. Wolf, A. Gröber, T. Böllinghaus, and A. Kranzmann, "Corrosion fatigue of 1.4542 exposed to a laboratory saline aquifer water CCS-environment," *GHGT13*, November 2016, Lausanne, Switzerland.

[46] R. Cohen *et al.*, "Low-cycle fatigue behaviour of 316L-type stainless steel in chloride solutions," *Corrosion Science,* vol. 51, pp. 3014-3120, 2009.

[47] A. Pfennig, R. Wiegand, M. Wolf, and C. P. Bork, "Corrosion and corrosion fatigue of AISI 420C (X46Cr13) at 60 ℃ in CO_2-saturated artificial geothermal brine," *Corrosion Science*, vol. 68, pp. 134–143, 2013.

A. Pfennig was born in Büdelsdorf, Germany in April 1970. She studied minerology at the Rheinische Friedrich Wilhelms University Bonn, Germany, where she graduated in 1997. Her Ph.D. in the field of ceramic moulds for liquid metal casting was earned in 2001 from the Friedrich Alexander University of Erlangen, Germany. She then worked for Siemens Energy in charge of ceramic shields and transferred to Berlin in 2008 where she currently teaches material science for engineering students at the Applied University Berlin, HTW. A. Pfennig research interest and expertise is in the field of corrosion fatigue of materials at high temperature and high pressure simulating geothermal environments.

A. Kranzmann was born in Bad-Bibra, Germany in 1956. He studied physics at the University of Cologne, Germany and finished his Ph.D. 1988 in the field of metallurgy at the MPI for metals research, Germany, where he worked from 1986-1991. He then transferred to ABB AG in Heidelberg as head of section in charge of materials and surface technology and later R&D coordination manager of ABB Germany until 2001. From then on and currently he is group leader "microstructure of materials" at the BAM, Federal Institute for Research and Development. A. Kranzmann research interest and expertise is in the field of high temperature and gas corrosion, ageing of metals, experimental simulation of high-temperature processes and research of surface topology.